Antenna Design for the Localization of Pulmonary Lesions During Thoracoscopic Surgery

Alberto Battistel * **Peter P. Pott** ** **Eric D. Rößner** *** **Knut Möller** *

* *Institute of Technical Medicine (ITeM), Furtwangen University (HFU), Jakob-Kienzle-Strasse 17, 78054 Villingen-Schwenningen, Germany (e-mail: alberto.battistel@hs-furtwangen.de).*
** *Institute of Medical Device Technology, University of Stuttgart, Pfaffenwaldring 9, 70569 Stuttgart, Germany*
*** *Academic Thoracic Center Mainz, Division of Thoracic Surgery, University Medical Center of the JohannesGutenberg University Mainz, Langenbeckstraße 1, 55101 Mainz, Germany*

Abstract: Video-assisted thoracoscopic surgery (VATS) is the primary minimally invasive excise procedure for the diagnostics of pulmonary lesions. However, these lesions can be difficult to localize during the surgery as the lung collapses. Here we continue our study on the use of radio frequency technology directly during VATS as an intraoperative strategy for the location of pulmonary lesions. Finite Difference Time Domain (FDTD) simulations were used to compare a dipole and a bowtie antenna of different lengths. The results show that the bowtie antenna performs better than a dipole one, even if only marginally.

Keywords: pulmonary lesion; laparoscopy; microwave imaging; ultra-wideband (UWB); finite difference time domain (FDTD)

1. INTRODUCTION

Thoracic surgeon are frequently asked to minimal invasively excise small lung lesion for diagnostic or therapeutic reasons which is performed through video-assisted thoracoscopic surgery (VATS). The need for those procedures is increasing, due to the programmed follow ups of extrathoracic cancers and especially due to the upcoming lung cancer screening programs (Meyer et al., 2017).

Small nodules deep within the lung tissue are extremely challenging for VATS surgeons due to localization difficulties. The inability to localize these nodules visually or with the impaired possibilities of manual/digital palpation may lead to intraoperative conversion to a thoracotomy losing the main advantages of a VATS procedure like rapid recovery, less complications, and shorter hospital stay. As a solution for this localization problem, many strategies have been developed with none of them achieving a major practice change due to their complexities, associated risks, and cost.

These strategies include preoperative spiral computed tomography (CT) guided marking with metal guidewires (Kostrzewa et al., 2017), fiducial or dye (Keating and Singhal, 2016) as well as endobronchial markings with guidance under ENB (electromagnetic navigational bronchoscopy) (Zhao et al., 2016) and intraoperative cone beam CT guidewire marking (Uneri et al., 2013; Zhao et al., 2019).

The risks associated with these procedures can be pneumothorax and hemothorax due to guidewires insertion (Keating and Singhal, 2016). Also, complications can arise in case of dislodged or displaced of the guidewire and in the case of dye marking, the effectiveness of the preoperative technique highly depend on the type of dye and on the time lapse before the VATS (Keating and Singhal, 2016).

Intraoperative techniques such as ultrasound, fluorescence with CT, and molecular imaging, are more suitable than preoperative ones because they are less costly and invasive (Keating and Singhal, 2016).

The problem associated with the intraoperative location of pulmonary lesions is depicted in Figure 1. Part a) shows a schematic with the real position of the lesion as for example detected during CT. On the other hand Figure 1 b) displays the situation during a VATS where the lung is collapsed and the previous knowledge about the position of the lesion is not longer valid. In this case either the lesion was marked before VATS or it has to be localized during the surgery.

One possible solution beyond the existing techniques is to use radio frequency (RF) technology to individuate the lesion. This works by bringing an antenna in close proximity with the collapsed lung (Figure 1 c) (Battistel et al., 2021; Battistel and Möller, 2021a,b). This antenna should be mounted on a thoracoscopic tool to be used

⋆ This research was partially funded by BMBF grant number FKZ: 13FH5I05IA COHMED-DigiMed-OP and grant AIRLobe funded by "Innovative Projects" MWK-BW.

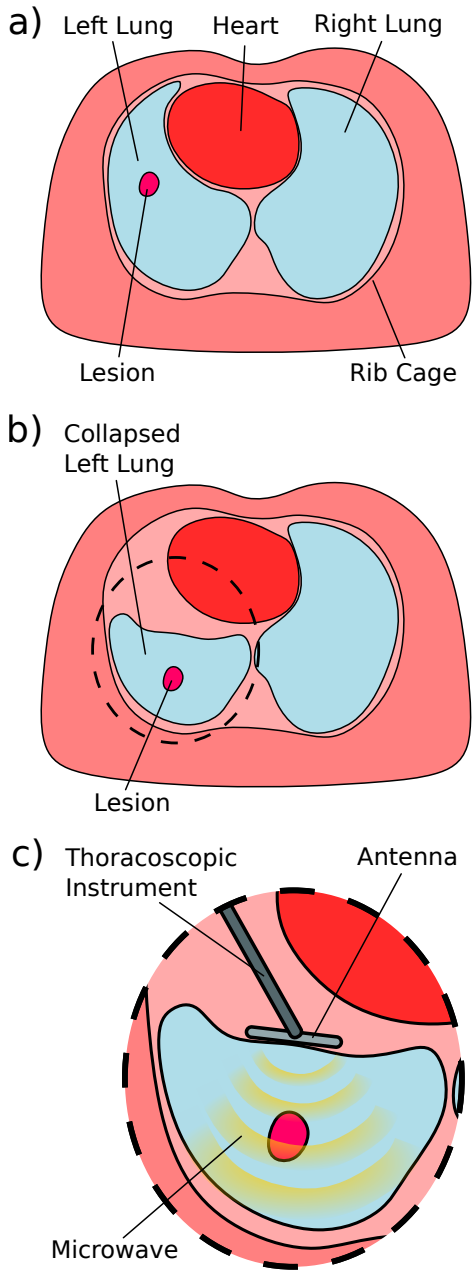

Fig. 1. Schematic of the thorax before and during thoracoscopy. a) Cross section of the chest. b) Cross section of the chest with the left lung collapsed and a new position for the lesion. c) Detail of a thoracoscopic tool with a microwave antenna illuminating the collapsed lung in proximity of the lesion to investigate.

during the VAT in such a way that it can illuminate the lung directly without additional interferences from other organs and tissues (Battistel et al., 2021). Therefore its dimensions are critical. The antenna should work in the microwave range and specifically at frequencies which can give a wavelength is in the range of mm or cm in the lung tissue. In our preliminary works 600 MHz was found as an optimal frequency (Battistel et al., 2021; Battistel and Möller, 2021b). At this frequency a microwave image constructed though delay-and-sum beamforming could show the position of a lesion up to 10 cm of depth (Battistel et al., 2021; Battistel and Möller, 2021b).

Microwave imaging has a long history of applications for breast cancer detection (Fear et al., 2002) and it can be, therefore, a suitable candidate also for the detection of pulmonary cancers and lesions.

In this contribution we compare two different kind of antennas through numerical simulations: a dipole and a bowtie antenna. The main characteristic of the dipole antenna is its narrow bandwidth, while the bowtie is a broadband antenna, but contrary to the dipole has a larger shape. The length of the antennas was varied between 2 cm and 6 cm. This matches the half wavelength $\lambda/2$ at 600 MHz in the lung tissue ($\lambda = 6.81$ cm). The dipole antenna does not place any problem to be mounted on a laparoscopic instrument as it is composed by two metal sticks, however for the bowtie antenna we selected a width of 1 cm as this is a good compromise between size and bandwidth.

2. MATERIALS AND METHODS

The propagation of electromagnetic waves is described by Faraday's law (eq. 1), Ampère's circuital law (eq. 2), Gauss's law (eq. 3), and the nonexistence of a magnetic monopole (eq. 4) (Cheng, 1992).

$$\nabla \times E = -\frac{\partial B}{\partial t} \tag{1}$$

$$\nabla \times H = J + \frac{\partial D}{\partial t} \tag{2}$$

$$\nabla \cdot D = \rho_v \tag{3}$$

$$\nabla \cdot B = 0 \tag{4}$$

which are also known as the four Maxwell's equations and together with the constitutive relations:

$$D = \epsilon * E \tag{5}$$

$$B = \nu * H \tag{6}$$

$$J_c = \sigma * E \tag{7}$$

describe how the electric and the magnetic field E [V m^{-1}] and H [A m^{-1}] are interconnected through the electric displacement field D [C m^{-2}], the magnetic flux density B [T], their time derivatives, the volumetric charge density ρ_v [C m^{-3}], and the current density J [A m^{-2}]. This last one can be decomposed into the conductive current J_c and the surface current J_s.

The equations (5) to (7) link D, B, and J_c to the properties of the material in which the electromagnetic waves propagate. These are convolutional relations, $*$ is the convolution sign, as the dielectric permittivity ϵ [F m^{-1}], the magnetic permeability ν [H m^{-1}], which is usually taken as zero for biological materials, and the conductivity σ [Ω m] are time, *viz.* frequency, dependent quantities.

The equations 1 - 7 can be solved using a Finite Difference Time Domain (FDTD) implementation which compute E and H at alternative time steps through finite differences on a staggered grid. This grid is also known as Yee cells (Yee, 1966). The solver used in this contribution for the simulations was gprMax version 3.1.5 (Warren et al., 2016; Giannakis and Giannopoulos, 2014) on a 3D space as schematized in Figure 2 a).

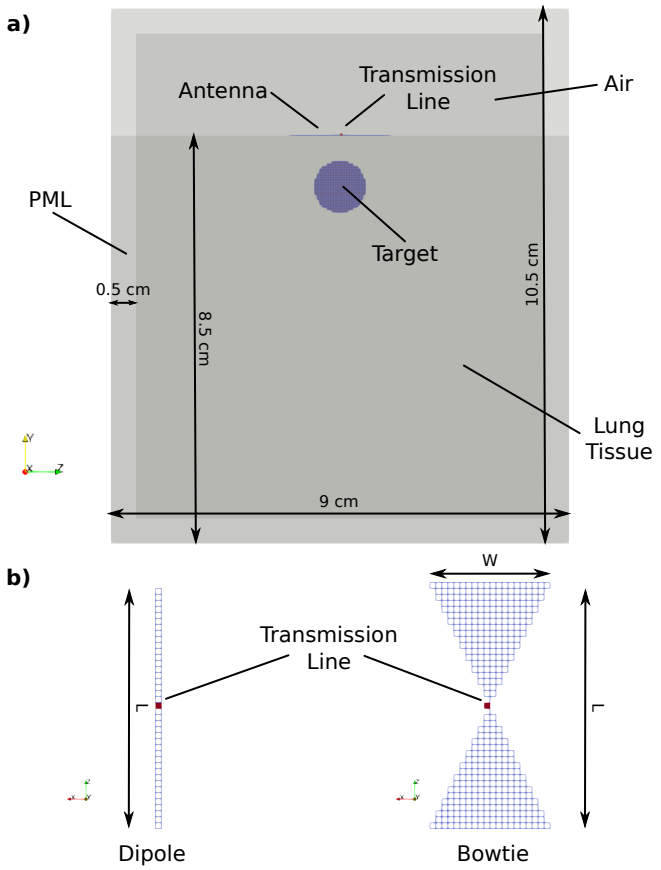

Fig. 2. Schematic of the simulation. a) Lateral view of the simulation domain with dimensions. b) Zoom in of the dipole and bowtie antennas.

An antenna of different lengths was simulated on the top of a half-space made of a material resembling lung tissue. The antenna was designed as two perfectly electric conductor patches aligned in the z direction made with the `#plate` or `#triangle` command depending on the shape of the antenna and the `pec` material identifier. The gap between the patches was one single cell wide where a transmission line element (`#transmission_line`) with a characteristic impedance of 50 Ω and polarized along the z direction was placed. Figure 2 b) shows the simulated structures for the two antennas.

Considering a relative permittivtiy of 52.8 at 600 MHz for the lung (Gabriel, 1996), the wavelength λ in the tissue is circa 6.8 cm. Therefore the total size of the antennas was taken between 2 cm and 6 cm which matches the $\frac{\lambda}{2}$ for a half-wave dipole.

The dimension of the computation domain were 7 cm, 10.5 cm and 9 cm for the x, y, and z direction. The lengths L of the antennas (Figure 2 b) were 2 cm to 6 cm. The width of the dipole and bowtie antenna was $W = 0.5$ mm and $W = 1$ cm.

Ten-cells wide perfectly matched layers (PML, `#PML`) as highlighted by darker areas in Figure 2 a) were used to truncate the computation in all the directions. A 0.5 mm voxel was used for the spacial discretization.

The dielectric permittivity ϵ_r and the conductivity σ for lung tissue were taken from the *Deflated Lung* material

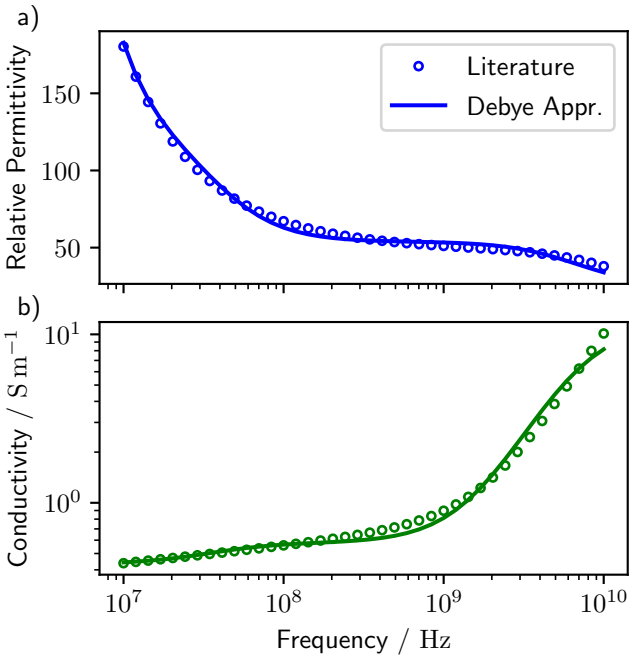

Fig. 3. Comparison between the relative dielectric permittivity ϵ_r (a) and the conductivity σ (b) derived from literature fitted with 3 Debye relaxation constants.

library (Gabriel, 1996). The analytical function describing the complex permittivity was taken from (Gabriel, 1996; Gabriel et al., 1996). The dispersive properties of the lung material were approximated by fitting the complex permittivity with 3 Debye relaxations functions with a particle swarming optimization algorithm (Kelley et al., 2007). These were then incorporated into the simulations with the commands `#material` and `#add_dispersion_debye`.

The relative permittivity used was 24.6, the three permittivity deltas were 9490, 69.3 and 29.2, and the three time constants $1.93 \cdot 10^{-7}$ s, $4.26 \cdot 10^{-9}$ s and $2.33 \cdot 10^{-11}$ s.

The maximal and mean relative error with three relaxation constants was 11.8 % and 3.9 % for the relative permittivity, 24.1 % and 5.9 % for the conductivity, and 5.4 % and 1.9 % for the wavelength.

To simulate a pulmonary lesion a metallic spherical target of 1 cm in diameter was placed below the antenna at different depth between 1 cm and 5 cm. This was designed with the command `#sphere` and the `pec` material identifier. Although dielectric parameters for cancerous lung tissue were reported (Wang et al., 2014) these go only up to 100 MHz and do not allow to estimate proper dispersive properties, that is the position and intensity of the relaxations in the frequency range used here. Therefore only perfectly metallic targets were simulated. As a perfect metal offers the maximal reflectivity, these targets give the upper limit for detectability.

The transmission line was powered by an excitation pulse centered at 600 MHz, as this was found to be the best frequency in our preliminary analysis (Battistel et al., 2021; Battistel and Möller, 2021b), with a 1 V-amplitude derivative of Gaussian function (`gaussiandot` in gprMax).

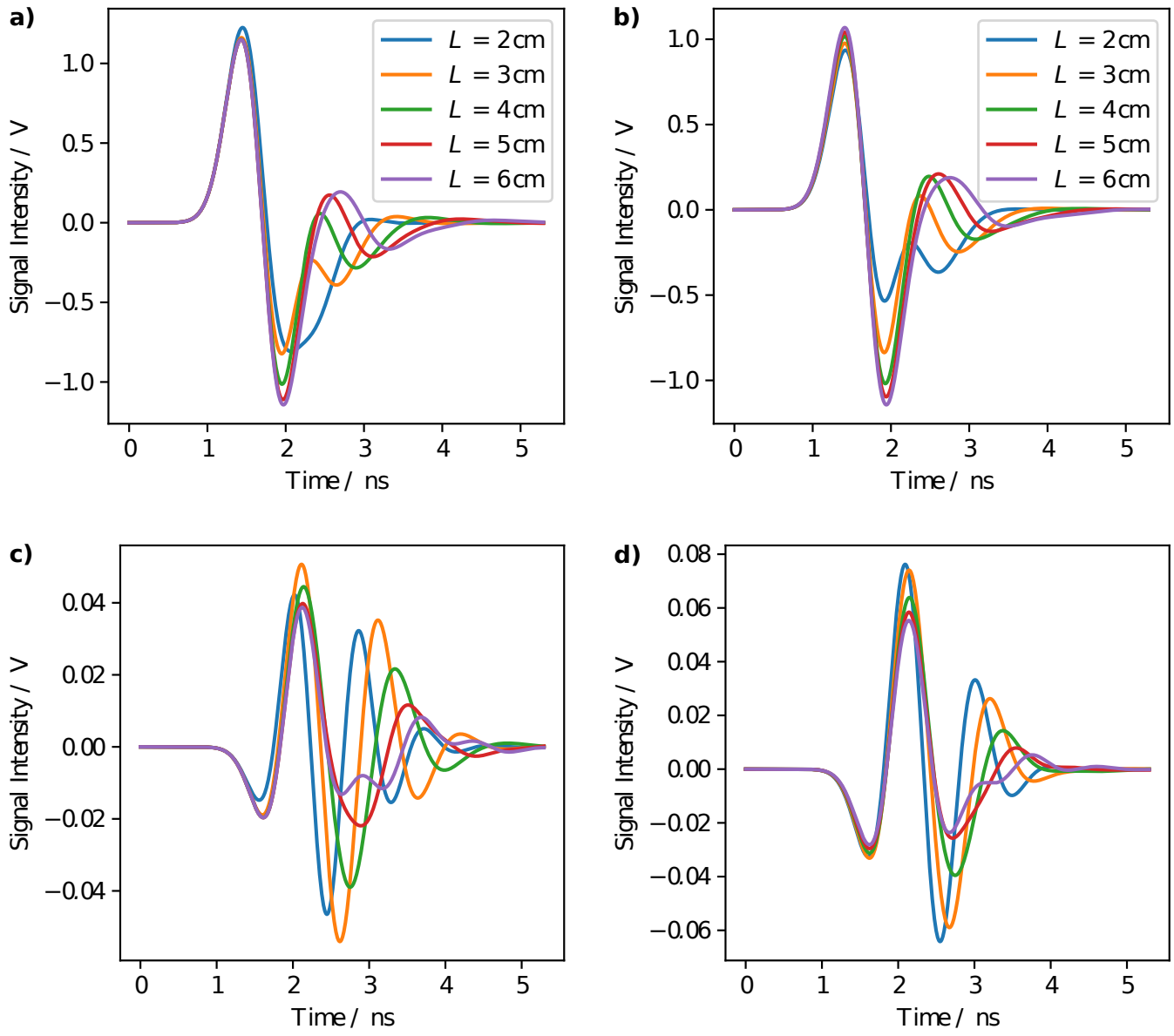

Fig. 4. Waveforms for the dipole (a and c) and bowtie (b and d) antennas without target (a and b) and difference between the waveform with and without the target (c and d).

3. RESULTS AND DISCUSSIONS

3.1 Waveforms comparison

Figure 4 a) and b) shows the waveforms for the dipole and bowtie antenna of different lengths L without any target present. They have similar shape and in both cases the main differences appear after circa 1.7 ns. The intensity of the first minimum at 2 ns follows a trend. In fact, with shorter antennas the minimum is more shallow. Opposite behavior appears for the second maximum. However, there are differences between the two different kinds of antenna. These differences are stronger for the shortest antenna length as the waveform for the dipole for $L = 2$ cm does not show a clear maximum between 2 ns and 3 ns where a clear peak is visible in Figure 4 c) for the same length.

To highlight the performances of the different antenna kinds, in Figure 4 c) and d) the difference between the waveforms with a target present at a depth of 1 cm and without any target are reported. For both antennas the waveforms display a sequence of maxima and minima where in both cases the first maxima and of the second minima are the most intense. The maximal intensity is circa 15 times lower than the maximal intensity of the signals of Figure 4 a) and c) with a small difference between the antennas: the maximal intensity of the difference is higher: it was circa 75 mV for the bowtie antenna against circa 50 mV for the dipole. This gives a first suggestion that the dipole antenna perform better as it recover a stronger signal from the metallic target.

3.2 Comparison through Euclidian distance

A clear trend which follows the antenna lengths for both antennas type is not visible as not only the intensity of the peaks change but also their relative position.

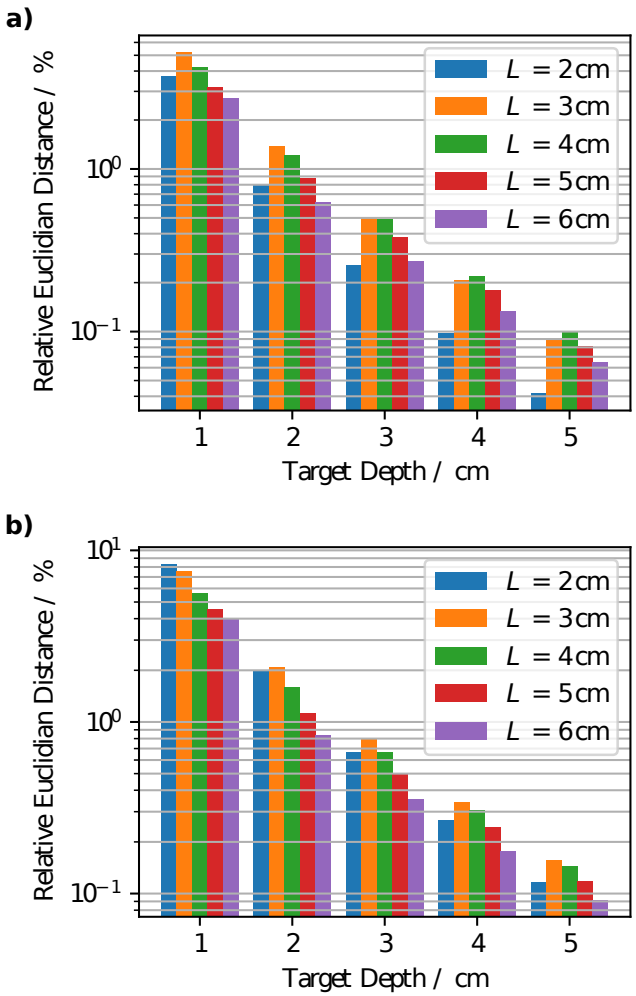

Fig. 5. Normalized Euclidian distance ($\tilde{d}$) for a 1 cm target at different depths for different length of the dipole antenna.

We define the Euclidian distance d_l (V) between a waveform w_l (V) simulated in presence of a target as:

$$d_l = \sqrt{\sum_{i=1}^{n} \left(w_l(t_i) - w_0(t_i)\right)^2} \tag{8}$$

where w_0 is the waveform for the same antenna length, but without target as figure of merit. We normalize the Euclidian distance with:

$$\tilde{d_l} = \frac{d_l}{\|w_0(t)\|_2} \tag{9}$$

where $\|\cdot\|_2$ is the Euclidean norm, also called the L_2 norm, of the waveform without target. If the target produces no effect on the waveform w_1 compared to the waveform without target w_0 then $\tilde{d_1}$ is zero. On the other hand, $\tilde{d_l} > 1$ means that w_l is more different, distant in an Euclidian sense, from w_0 than w_0 is from a flat line.

Figure 5 a) shows the normalized Euclidian distances $\tilde{d}$ for different dipole antenna sizes L and target depths and Figure 5 b) shows the same for the bowtie antenna.

As expected, for both antennas, $\tilde{d}$ decreases with increasing target depth as the intensity of the reflected wave quickly decrease with the distance of the scattering object and therefore the waveform recorded at the antenna is more and more similar to that without any target.

For the dipole antenna and a target depth of 1 cm $\tilde{d_l}$ was between 3 % and 5 % while it went to 0.04 % to 0.1 % for a target depth of 5 cm. The trend is not so clear if we consider the different antenna lengths. In particular, between 1 cm and 3 cm the best performances, larger $\tilde{d_l}$, were given by the dipole with a length of 3 cm followed by the dipole with length 4 cm. For the deepest targets, instead, the best antenna was that with $L = 4$ cm. The worst dipole was that with $L = 6$ cm up to $L = 3$ cm and then the one with $L = 1$ cm.

The normalized Euclidian distance $\tilde{d_l}$ for the bowtie antenna (Figure 5 b) goes from between 4 % and 8 % for a target depth of 1 cm to between 0.09 % and 0.15 % for a target depth of 5 cm. These values were higher than for the dipole antenna as already suggested from Figure 4 c) and d). Also, the relative trend between different antenna lengths was different. In fact, with 1 cm of target depth the best antenna was that with a length of 2 cm followed by that of 3 cm. However, at higher depths the best antenna was that with $L = 3$ cm followed by that with $L = 4$ cm, except for the depth of 2 cm, where the second best dipole was that with $L = 2$ cm. On the other hand the worst antenna was consistently the dipole with $L = 6$ cm.

Considering the results for both antennas the length of the antenna should be between 3 cm and 4 cm. This value matches the half wavelength for an electromagnetic wave of 600 MHz ($\lambda = 6.81$ cm).

4. CONCLUSIONS

In this article two different antenna types were investigated by numerical analysis for the localization of lung lesion by microwave illumination. The study compared a dipole and a bowtie antenna of different length through finite difference time domain (FDTD) simulations to see which design shows the larger variation in signal when a fictional lung lesion was present under the antenna. The antenna was designed to operate directly in contact with lung tissue as it is the case during a thoracoscopic surgery at the frequency of 600 MHz since this value gave the best performances in our preliminary study (Battistel et al., 2021; Battistel and Möller, 2021b).

It was found that the waveform given by the two kinds of antenna were similar but the bowtie antenna performed better than the dipole antenna for all the antenna lengths. In fact, the backscattering signal intensity was one and half time larger. However, there is not a clear winner regarding the antenna length. In fact, for the shallowest target (1 cm) the shortest antenna showed the best performances, while for all the other target depths the best length was 4 cm.

This indicates that broadband antennas have better capabilities for microwave imaging. Nevertheless further im-

provements are still necessary. In fact here only a perfectly conducting target was considered, which represents the best condition. Also, shallow targets produced a variation on the antenna waveform of some 4 % to 8 %, but deeper targets displayed a progressively weaker influence which could be lost into the environmental noise.

Further considerations are also necessary concerning the sizing of the antenna and the materials used. In fact, to be employed during a video-assisted thoracoscopic surgery, the antenna needs to be small enough to pass through the small incisions made on the chest wall or at least to be foldable so to deploy its full size once inside the thoracic cage. Furthermore, regarding the materials that house the antenna, they need to be suitable for a medical environment where frequent sterilizations are necessary.

Different strategies can be employed to improve the signal quality as for example use spacing materials with tuned dielectric properties and change the shape of the waveform used. Finally, we foresee testing with phantoms and biological tissues to take into account the noise level and the real effective variability in dielectric properties even in the same organ.

REFERENCES

Battistel, A. and Möller, K. (2021a). Ultra-Wideband Localization of Pulmonary Nodules during Thoracoscopic Surgery. *Engineering Proceedings*, 6(1), 4. doi:10.3390/I3S2021Dresden-10095.

Battistel, A. and Möller, K. (2021b). Ultra-wideband Localization of Pulmonary Nodules During Thoracoscopic Surgery. In T. Jarm, A. Cvetkoska, S. Mahnič-Kalamiza, and D. Miklavcic (eds.), *8th European Medical and Biological Engineering Conference*, IFMBE Proceedings, 1146–1155. Springer International Publishing, Cham. doi:10/gj3cn8.

Battistel, A., Pott, P.P., and Möller, K. (2021). Numerical Analysis of the Localization of Pulmonary Nodules during Thoracoscopic Surgery by Ultra-Wideband Radio Technology. *Applied Sciences*, 11(9), 4282. doi:10/gj3cjt.

Cheng, D.K. (1992). *Fundamentals of Engineering Electromagnetics*. Prentice Hall, 1st edition.

Fear, E., Li, X., Hagness, S., and Stuchly, M. (2002). Confocal microwave imaging for breast cancer detection: Localization of tumors in three dimensions. *IEEE Transactions on Biomedical Engineering*, 49(8), 812–822. doi:10/fmpkxb.

Gabriel, C. (1996). Compilation of the Dielectric Properties of Body Tissues at RF and Microwave Frequencies. Technical report, King's Coll London (United Kingdom) Dept of Physics.

Gabriel, S., Lau, R.W., and Gabriel, C. (1996). The dielectric properties of biological tissues: III. Parametric models for the dielectric spectrum of tissues. *Physics in Medicine and Biology*, 41(11), 2271–2293. doi:10/dkcsq8.

Giannakis, I. and Giannopoulos, A. (2014). A Novel Piecewise Linear Recursive Convolution Approach for Dispersive Media Using the Finite-Difference Time-Domain Method. *IEEE Transactions on Antennas and Propagation*, 62(5), 2669–2678. doi:10.1109/TAP.2014.2308549.

Keating, J. and Singhal, S. (2016). Novel Methods of Intraoperative Localization and Margin Assessment of Pulmonary Nodules. *Seminars in Thoracic and Cardiovascular Surgery*, 28(1), 127–136. doi:10/gg238t.

Kelley, D.F., Destan, T.J., and Luebbers, R.J. (2007). Debye Function Expansions of Complex Permittivity Using a Hybrid Particle Swarm-Least Squares Optimization Approach. *IEEE Transactions on Antennas and Propagation*, 55(7), 1999–2005. doi:10/bqh2dr.

Kostrzewa, M., Kara, K., Rathmann, N., Tsagogiorgas, C., Henzler, T., Schoenberg, S.O., Hohenberger, P., Diehl, S.J., and Roessner, E.D. (2017). Computed Tomography-Assisted Thoracoscopic Surgery: A Novel, Innovative Approach in Patients With Deep Intrapulmonary Lesions of Unknown Malignant Status. *Investigative Radiology*, 52(6), 374–380. doi:10/f99dj4.

Meyer, M., Vliegenthart, R., Henzler, T., Buergy, D., Giordano, F.A., Kostrzewa, M., Rathmann, N., Brustugun, O.T., Crino, L., Dingemans, A.M.C., Dusmet, M., Fennell, D., Grunenwald, D., Huber, R.M., Moniuszko, M., Mornex, F., Papotti, M., Pilz, L., Senan, S., Syrigos, K., Pérol, M., Gray, J.E., Schabel, C., van Meerbeeck, J.P., van Zandwijk, N., Zhou, C.C., Manegold, C., Voigt, W., and Roessner, E.D. (2017). Management of Progressive Pulmonary Nodules Found during and outside of CT Lung Cancer Screening Studies. *Journal of Thoracic Oncology: Official Publication of the International Association for the Study of Lung Cancer*, 12(12), 1755–1765. doi:10.1016/j.jtho.2017.09.1956.

Uneri, A., Nithiananthan, S., Schafer, S., Otake, Y., Stayman, J.W., Kleinszig, G., Sussman, M.S., Prince, J.L., and Siewerdsen, J.H. (2013). Deformable registration of the inflated and deflated lung in cone-beam CT-guided thoracic surgery: Initial investigation of a combined model- and image-driven approach. *Medical Physics*, 40(1), 017501. doi:10/gkrwjv.

Wang, J.R., Sun, B.Y., Wang, H.X., Pang, S., Xu, X., and Liu, Q. (2014). Experimental Study of Dielectric Properties of Human Lung Tissue in Vitro. *Journal of Medical and Biological Engineering*, 34(6), 598–604. doi:10/ggnd4s.

Warren, C., Giannopoulos, A., and Giannakis, I. (2016). gprMax: Open source software to simulate electromagnetic wave propagation for Ground Penetrating Radar. *Computer Physics Communications*, 209, 163–170. doi:10.1016/j.cpc.2016.08.020.

Yee, K. (1966). Numerical solution of initial boundary value problems involving maxwell's equations in isotropic media. *IEEE Transactions on Antennas and Propagation*, 14(3), 302–307. doi:10/b8dmtt.

Zhao, Z.R., Lau, R.W.H., and Ng, C.S.H. (2016). Hybrid theatre and alternative localization techniques in conventional and single-port video-assisted thoracoscopic surgery. *Journal of Thoracic Disease*, 8(Suppl 3), S319–327. doi:10/gkrwjr.

Zhao, Z.R., Lau, R.W.H., Yu, P.S.Y., and Ng, C.S.H. (2019). Devising the guidelines: The techniques of pulmonary nodule localization in uniportal video-assisted thoracic surgery-hybrid operating room in the future. *Journal of Thoracic Disease*, 11(Suppl 16), S2073–S2078. doi:10/gkrwjt.